

Cluster-guided Asymmetric Contrastive Learning for Unsupervised Person Re-Identification

Mingkun Li, Chun-Guang Li, *Senior Member, IEEE*, and Jun Guo

Abstract—Unsupervised person re-identification (Re-ID) aims to match pedestrian images from different camera views in an unsupervised setting. Existing methods for unsupervised person Re-ID are usually built upon the pseudo labels from clustering. However, the result of clustering depends heavily on the quality of the learned features, which are overwhelmingly dominated by colors in images. In this paper, we attempt to suppress the negative dominating influence of colors to learn more effective features for unsupervised person Re-ID. Specifically, we propose a Cluster-guided Asymmetric Contrastive Learning (CACL) approach for unsupervised person Re-ID, in which clustering result is leveraged to guide the feature learning in a properly designed asymmetric contrastive learning framework. In CACL, both instance-level and cluster-level contrastive learning are employed to help the siamese network learn discriminant features with respect to the clustering result within and between different data augmentation views, respectively. In addition, we also present a cluster refinement method, and validate that the cluster refinement step helps CACL significantly. Extensive experiments conducted on three benchmark datasets demonstrate the superior performance of our proposal.

Index Terms—Unsupervised Person Re-Identification, Asymmetric Contrastive Learning, Cluster Refinement.

I. INTRODUCTION

UNSUPERVISED person Re-identification (Re-ID) aims to match pedestrian images from different camera views in unsupervised setting without demanding massive labelled data, and has attracted increasing attention in computer vision and pattern recognition community in recent years [1]. The great challenge we face in unsupervised person Re-ID is to tackle heavy variations from different viewpoints, varying illuminations, changing weather conditions, cluttered background and etc., without supervision labels.

Recently, existing methods for unsupervised person Re-ID are usually built on exploiting weak supervision information (e.g., pseudo labels) from clustering. For example, MMT [2] uses DBSCAN [3] algorithm to generate pseudo labels and exploit the pseudo labels to train two networks. HCT [4] uses a hierarchical clustering algorithm to gradually assign pseudo labels to the training samples during the training stage. SSG [5] uses k -means on training samples with multi-views. However, the performance of these methods heavily relies on the quality of the pseudo labels, which directly depends on the feature representation of the input images.

M. Li, C.-G. Li and J. Guo are with the School of Artificial Intelligence, Beijing University of Posts and Telecommunications, Beijing, 100876 P.R. China e-mail: {mingkun.li, lichunguang, guojun}@bupt.edu.cn.

Chun-Guang Li is the corresponding author.

Manuscript received xx, 2021; revised xx, xxxx.

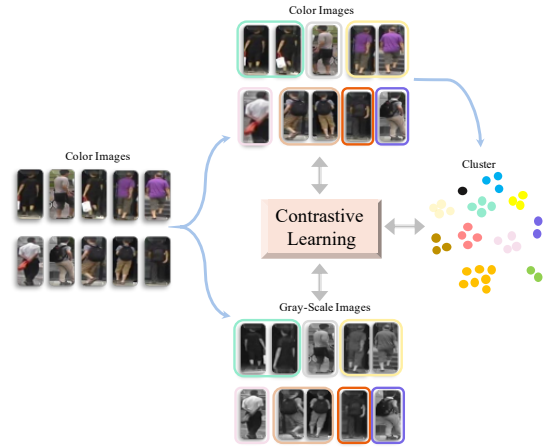


Fig. 1. Illustration for basic idea of our proposal. We attempt to leverage the clustering information into contrastive learning to find more effective features by exploring the invariance between color images and gray-scale images.

More recently, contrastive learning is applied to perform feature learning in unsupervised setting, e.g., [6], [7], [8], [9], [10]. The primary idea in these methods is to learn some invariance in feature representation with self-supervised mechanism based on data augmentation. In SimCLR [8], each sample and its multiple augmentations are treated as positive pairs, and the rest of the samples in the same batch are treated as negative pairs and, a contrastive loss is used to distinguish the positive and negative samples to prevent the model from falling into a trivial solution. We note that SimCLR requires to use a large batch size, e.g., 256 ~ 4096, to contain enough negative samples for effectively training the networks. In BYOL [10] and SimSiam [9], a predictor layer is used to prevent feature collapse without using negative samples. In InterCLR [6] and SwAV [7], clustering is used to prevent the feature collapse. In particular, in SwAV [7], a scalable online clustering loss is proposed to train the siamese network with multi-crop data augmentation; whereas in InterCLR [6], a MarginNCE loss is proposed to enhance the discriminant power. While promising performance has been reported on ImageNet [11], however, these contrastive learning methods are not suitable for unsupervised person Re-ID due to serious feature collapse.

In this paper, we attempt to leverage cluster information into contrastive learning to develop an effective framework for unsupervised person Re-ID. We notice that the performance of person Re-ID depends heavily on the effectiveness of the learned features. However, the learned features are overwhelm-

ingly dominated by the colors in pedestrian images (such as the clothing color and background color), especially in the unsupervised setting. For example, the pedestrian images with similar color clothes often have smaller distances in feature space, which may result in mistakes in clustering, and the mistakes in clustering may further bring wrong guidance to the pseudo labels for training the network. Although colors are important feature to match pedestrian images for person Re-ID, it may also become an obstacle to learn more subtle and effective texture features that are important fine-level cues for person Re-ID. Thus it is desirable to learn more robust and discriminating features that can resist dominant colors for person Re-ID task.

Unfortunately, it is quite challenging to properly suppress the negative impact of colors for learning more effective fine-grain level features without loss of discriminant information. For example, directly using random color changing (i.e., color-jitter [12]) for data augmentation in contrastive training may damage the consistency in color distribution, not that helpful to gain generalization ability on unseen samples. To this end, in this paper, we propose a novel and effective framework for unsupervised person Re-ID, termed Cluster-guided Asymmetric Contrastive Learning (CACL), in which clustering information is properly incorporated into contrastive learning to learn robust and discriminant features while suppressing dominant colors, as illustrated in Fig. 1. To be specific, we explore supervision information from the perspective of suppressing colors in the framework of cluster-guided contrastive learning, in which the samples in asymmetric views of specifically designed data augmentations (e.g., color images vs. gray-scale images) as shown in Fig. 2—are exploited to provide strong supervision to impose invariance in feature learning. By integrating the clustering results into contrastive learning, the proposed framework is able to avoid feature collapse. By suppressing dominant colors, the proposed framework is able to effectively learn robust and discriminating features other than colors. In addition, we also present a simple but effective cluster refinement method to improve the clustering result and thus further enhancing the contrastive learning. We conduct extensive experiments on three benchmark datasets, and experimental results validate the effectiveness of our proposal.

Paper Contributions. The contributions of the paper are highlighted as follows.

- 1) We propose an effective unsupervised framework that leverages clustering information into contrastive learning while suppressing the dominant colors in images to learn fine-grained features.
- 2) We propose a novel cluster-level loss function to perform inter-views and intra-view contrastive learning that can effectively exploit the cluster-level hidden information from different data augmentation views.
- 3) We also present a cluster refinement method and verify that the refined clustering information helps the contrastive learning framework significantly.

The remainder of this paper is organized as follows. Section II describes the relevant work. Section III presents our

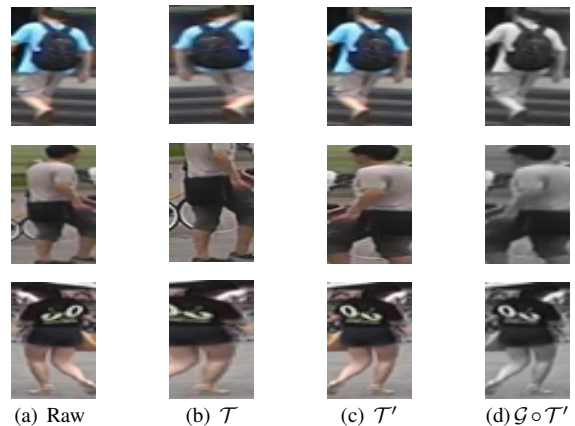


Fig. 2. Illustration for the raw images and the augmented images. The first column shows the raw images. The middle two columns show the images generated with transforms $\mathcal{T}(\cdot)$ and $\mathcal{T}'(\cdot)$. The last column shows the corresponding gray-scale images which are generated with both transform $\mathcal{T}'(\cdot)$ and color-to-grayscale transform $\mathcal{G}(\cdot)$, i.e., $\mathcal{G} \circ \mathcal{T}'(\cdot)$.

proposal. Section IV shows experiments and Section V gives the conclusions.

II. RELATED WORK

A. Unsupervised Person Re-identification

Person Re-ID aims to find specific pedestrians from videos or images according to targets. For the increasing demand in real life and avoiding the high consumption of labeling datasets, unsupervised person Re-ID has become popular in recent years [1]. The existing unsupervised person Re-ID methods can be divided into two categories: a) unsupervised domain adaptation methods, that need labeled source dataset and unlabeled target dataset [13], [14], [15], [16]; and b) pure unsupervised methods, that need with only unlabeled dataset [17], [18], [19], [20].

The unsupervised domain adaptation methods train the network with the help of labeled datasets, and transfer the network to unlabeled datasets by reducing the gap between two datasets. For example, [21] proposed to align the second-order statistics of the distributions in the two domains through linear transformations to reduce the domain shift; [17] proposed a combined loss function to co-train with samples from the source and target domains and the merging memory bank; [22] proposed to maximize the inter-domain classification loss and minimize the intra-domain classification loss to learn domain robust features. However, unsupervised domain adaptation methods are limited by the requirement of the target dataset having close distribution to the source dataset.

Most purely unsupervised person Re-ID methods rely on the pseudo labels to train the network. For example, HCT [4] uses hierarchical clustering to generate pseudo labels and train the convolution neural network for feature learning; [23] assigns multiple labels to samples and proposes a new loss function for multi-label training. Note that the quality of the pseudo labels relies on the feature representation of the input images. However, in the early stage, the feature representation is not good enough to generate high-quality pseudo labels, and thus

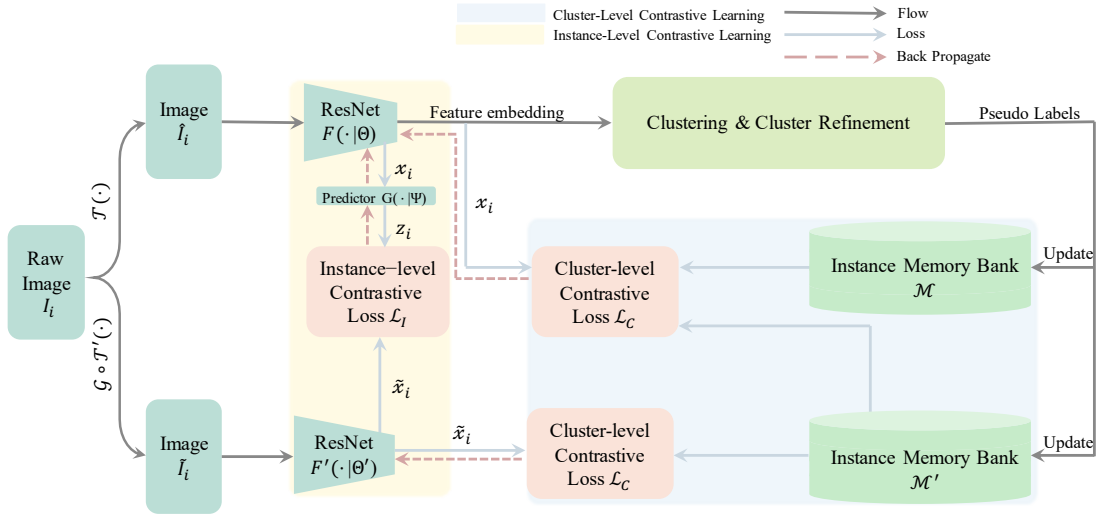


Fig. 3. Illustration for our proposed Cluster-guided Asymmetric Contrastive Learning (CACL) framework. After training, we keep only the ResNet $F(\cdot|\Theta)$ in the first branch for inference and use the feature x_i for testing.

the low-quality pseudo labels will contaminate the network training. Therefore, it is needed to design a cluster refinement method to improve the clustering quality before feeding the pseudo labels to train the network.

B. Contrastive Learning

In recent years, with the development and application of the siamese network, contrastive learning began to emerge in the field of unsupervised learning. Contrastive learning aims at learning good image representation. It learns invariance in features by manipulating a set of positive samples and negative samples with data augmentation.

The existing methods for contrastive learning can be further categorized to: a) instance-level methods [8], [9], [24], [25], [10] and b) cluster-level methods [7], [6], [26]. Instance-level methods regard each image as an individual class and consider two augmented views of the same image as positive pairs and treat others in the same batch (or memory bank) as negative pairs. For example, SimCLR [8] regards samples in the current batch as the negative samples; MoCo [27] uses a dictionary to implement contrastive learning, which converts one branch of the contrastive learning into a momentum encoder; SimSiam [9] proposed a stop-gradient method that can train the siamese network without negative samples. Cluster-level methods regard the samples in the same clusters as positive samples and other samples as negative samples. For example, in [6] InfoNCE loss is combined with MarginNCE loss to attract positive samples and repelled negative samples; in [7] multi-crop data augmentation is used to enhance the robustness of the network and a scalable online clustering method is proposed to explore the inter-invariance of clusters; in [26] weights-sharing deep neural networks are used to extract features from sample pairs with different data augmentations, and contrastive clustering is performed with respect to both the features in the row and column spaces.

However, in the unsupervised setting, the instance-level contrastive learning methods simply make each sample in-

dependently repel each other, which will undoubtedly ignore the cluster information. In contrast, cluster-level contrastive learning can effectively mine cluster information, but it relies heavily on the clustering result. Unfortunately, in the early training stage, the features are not good enough to yield good clustering result. Thus, an effective way to train the network by combining both the two lines of contrastive learning methods is needed.

In this paper, we attempt to bridge the two lines of contrastive learning methods into a unified framework to form effective mutual learning and joint training: a) the instance-level contrastive learning helps training the network to perform feature learning—especially in the early training stage; meanwhile b) the cluster-level contrastive learning helps training the network—especially when the quality of the clustering has been improved. In this way, the self-supervision information imposed by data augmentation and the weak supervision information obtained from clustering can be fully exploited without the need to use negative samples pairs.

III. OUR PROPOSAL: CLUSTER-GUIDED ASYMMETRIC CONTRASTIVE LEARNING (CACL)

This section presents our proposal—Cluster-guided Asymmetric Contrastive Learning (CACL) approach for unsupervised person Re-ID.

For clarity, we show the architecture of our proposed CACL in Fig. 3. Overall, our CACL is a siamese network, which consists of two branches of backbone networks $F(\cdot|\Theta)$ and $F'(\cdot|\Theta')$ without sharing parameters, where Θ and Θ' are the parameters in the two networks, respectively, and a predictor layer $G(\cdot|\Psi)$ is added after the first branch, where Ψ denotes the parameters in the predictor layer. The backbone networks $F(\cdot|\Theta)$ and $F'(\cdot|\Theta')$ are implemented¹ via ResNet-50 [28] for feature learning.

¹It also works if the backbone networks other than ResNet-50 are used.

Given an unlabeled image dataset $\mathcal{I} = \{I_i\}_{i=1}^N$ consisting of N samples. For an input image $I_i \in \mathcal{I}$, we generate two samples \hat{I}_i and \tilde{I}_i via different data augmentation strategies as the inputs of the two branches, respectively, in which $\hat{I}_i = \mathcal{T}(I_i)$ and $\tilde{I}_i = \mathcal{G}(\mathcal{T}'(I_i))$, where $\mathcal{T}(\cdot)$ and $\mathcal{T}'(\cdot)$ denote two different transforms and $\mathcal{G}(\cdot)$ denotes the operation to transform color image into gray-scale image. For simplicity, we denote the output features of the first network branch and the second network branch as \mathbf{x}_i and $\tilde{\mathbf{x}}_i$, and denote the output of the predictor layer in the first branch as \mathbf{z}_i , respectively, where $\mathbf{x}_i, \tilde{\mathbf{x}}_i, \mathbf{z}_i \in \mathbb{R}^D$.

The clustering result of the output features $\mathcal{X} := \{\mathbf{x}_1, \dots, \mathbf{x}_N\}$ from the first network branch is used to generate the pseudo labels $\mathcal{Y} := \{\mathbf{y}_1, \dots, \mathbf{y}_N\}$. We exploit the pseudo labels to leverage the cluster information into the contrastive learning. Specifically, in the training stage, the two network branches $F(\cdot|\Theta)$ and $F'(\cdot|\Theta')$ are trained with the augmented samples without sharing parameters, and the pseudo labels \mathcal{Y} are used to guide the training of both network branches.

In ACL, we use instance memory banks $\mathcal{M} = \{v_i\}_{i=1}^N$ and $\tilde{\mathcal{M}} = \{\tilde{v}_i\}_{i=1}^N$ where $v_i, \tilde{v}_i \in \mathbb{R}^D$ to store the outputs of two branches, respectively. Both instance memory banks \mathcal{M} and $\tilde{\mathcal{M}}$ are initialized with $\mathcal{X} := \{\mathbf{x}_1, \dots, \mathbf{x}_N\}$ and $\tilde{\mathcal{X}} := \{\tilde{\mathbf{x}}_1, \dots, \tilde{\mathbf{x}}_N\}$, which are the outputs of the network branches $F(\cdot|\Theta)$ and $F'(\cdot|\Theta')$ pre-trained on ImageNet, respectively.

A. Cluster-guided Contrastive Learning

At beginning, we pre-train the two network branches $F(\cdot|\Theta)$ and $F'(\cdot|\Theta')$ on ImageNet [11], and use the features from the first network branch $F(\cdot|\Theta)$ to yield m clusters, which are denoted as $\mathcal{C} := \{\mathcal{C}^{(1)}, \mathcal{C}^{(2)}, \dots, \mathcal{C}^{(m)}\}$. The clustering result is used to form pseudo labels to train the cluster-guided contrastive learning module.

To exploit the label invariance between the two augmented views and leverage the cluster structure, we employ two types of contrastive losses: a) instance-level contrastive loss, denoted as \mathcal{L}_I , and b) cluster-level contrastive loss, denoted as \mathcal{L}_C .

Instance-Level Contrastive Loss. To match the feature outputs \mathbf{z}_i and $\tilde{\mathbf{x}}_i$ of the two network branches at instance-level, similar to [8], [10], we introduce the negative cosine similarity of the prediction outputs \mathbf{z}_i in the first branch and the feature output of the second branch $\tilde{\mathbf{x}}_i$ to define an instance-level contrastive loss \mathcal{L}_I as follows:

$$\mathcal{L}_I := -\frac{\mathbf{z}_i^\top \tilde{\mathbf{x}}_i}{\|\mathbf{z}_i\|_2 \|\tilde{\mathbf{x}}_i\|_2}, \quad (1)$$

where $\|\cdot\|_2$ is the ℓ_2 -norm.

Cluster-Level Contrastive Loss. To leverage the cluster structure to further explore the hidden information from different views, we propose a cluster-level contrastive loss \mathcal{L}_C , which is further divided into inter-views cluster-level contrastive loss and intra-views cluster-level contrastive loss.

- Inter-views Cluster-level contrastive loss, denoted as $\mathcal{L}_C^{(inter)}$, which is defined as:

$$\mathcal{L}_C^{(inter)} := -\frac{\mathbf{z}_i^\top \tilde{\mathbf{u}}_{\omega(I_i)}}{\|\mathbf{z}_i\|_2 \|\tilde{\mathbf{u}}_{\omega(I_i)}\|_2}, \quad (2)$$

where $\omega(I_i)$ is to find the cluster index ℓ for \mathbf{z}_i , and $\tilde{\mathbf{u}}_\ell$ is the center vector of the ℓ -th cluster in which $\tilde{\mathcal{U}} := \{\tilde{\mathbf{u}}_1, \dots, \tilde{\mathbf{u}}_m\}$ and the cluster center $\tilde{\mathbf{u}}_\ell$ is defined as

$$\tilde{\mathbf{u}}_\ell = \frac{1}{|\mathcal{C}^{(\ell)}|} \sum_{I_i \in \mathcal{C}^{(\ell)}} \tilde{v}_i, \quad (3)$$

where \tilde{v}_i is the instance feature of image \tilde{I}_i in the instance memory bank $\tilde{\mathcal{M}}$, $\mathcal{C}^{(\ell)}$ is the ℓ -th cluster. The inter-views cluster-level contrastive loss $\mathcal{L}_C^{(inter)}$ defined in Eq. (2) is used to reduce the discrepancy between the projection output \mathbf{z}_i of the first network branch and the cluster center $\tilde{\mathbf{u}}_\ell$ of the feature output of the second branch with the gray-scale view.

- Intra-views Cluster-level contrastive loss, denoted as $\mathcal{L}_C^{(intra)}$, which is defined as:

$$\mathcal{L}_C^{(intra)} = -(1 - q_i)^2 \ln(q_i) - (1 - \tilde{q}_i)^2 \ln(\tilde{q}_i), \quad (4)$$

where q_i and \tilde{q}_i are the softmax of the inner product of the network outputs and the corresponding instance memory bank, which are defined as

$$q_i = \frac{\exp(\mathbf{u}_{\omega(I_i)}^\top \mathbf{x}_i / \tau)}{\sum_{\ell=1}^{m'} \exp(\mathbf{u}_\ell^\top \mathbf{x}_i / \tau)}, \quad (5)$$

$$\tilde{q}_i = \frac{\exp(\tilde{\mathbf{u}}_{\omega(I_i)}^\top \tilde{\mathbf{x}}_i / \tau)}{\sum_{\ell=1}^{m'} \exp(\tilde{\mathbf{u}}_\ell^\top \tilde{\mathbf{x}}_i / \tau)}, \quad (6)$$

where \mathbf{u}_ℓ and $\tilde{\mathbf{u}}_\ell$ are the center vectors of the ℓ -th cluster for the first branch and the second branch, respectively, in which $\tilde{\mathbf{u}}_\ell$ is defined in Eq. (3) and \mathbf{u}_ℓ is defined as

$$\mathbf{u}_\ell = \frac{1}{|\mathcal{C}^{(\ell)}|} \sum_{I_i \in \mathcal{C}^{(\ell)}} v_i, \quad (7)$$

where v_i is the instance feature of image \hat{I}_i in the instance memory bank \mathcal{M} . Note that both \mathbf{x}_i and $\tilde{\mathbf{x}}_i$ share the same pseudo labels $\omega(I_i)$ from clustering. The intra-views cluster-level contrastive loss $\mathcal{L}_C^{(intra)}$ in Eq. (4) is used to encourage the siamese network to learn features with respect to the corresponding cluster center for the two branches, respectively.

Putting the loss functions in Eqs. (2) and (4) together, we have the cluster-level contrastive loss \mathcal{L}_C as follows:

$$\mathcal{L}_C := \mathcal{L}_C^{(inter)} + \mathcal{L}_C^{(intra)}. \quad (8)$$

Remark 1. The cluster-level contrastive loss \mathcal{L}_C in Eq. (8) aims to leverage the clustering information to minimize the difference between the samples of the same cluster from different augmentation views via $\mathcal{L}_C^{(inter)}$, and within the same augmentation view via $\mathcal{L}_C^{(intra)}$. This will help the siamese network to mine the hidden information brought by the basic augmented view in the first branch and the gray-scale augmented view in the second branch to prevent feature collapse to a trivial solution and impose the supervision information to learn features other than colors.

B. Clustering and Cluster Refinement

Note that the cluster-level contrast loss is greatly affected by the quality of the clustering result. When the clusters are noisy, it will cause negative effects on the training. To improve the quality of the clustering result, we propose a cluster refinement method which removes a proportion of noisy samples in larger clusters, helping the model to better learn the information at the cluster level.

For a cluster, we want to keep the samples with higher similarity and remove the samples with lower similarity. Given a set of raw clusters, denoted as $\{\mathcal{C}^{(1)}, \mathcal{C}^{(2)}, \dots, \mathcal{C}^{(m)}\}$, without loss of generality, we pick $\mathcal{C}^{(i)}$ to perform cluster refinement. At first, we obtain an over-segmentation of $\mathcal{C}^{(i)}$, i.e., $\mathcal{C}^{(i)}$ is further divided into $\{\mathcal{C}_1^{(i)}, \mathcal{C}_2^{(i)}, \dots, \mathcal{C}_{n_i}^{(i)}\}$. Then we perform cluster refinement according to the following criterion:

$$\text{if } D(\mathcal{C}_j^{(i)}|\mathcal{C}^{(i)}) < D(\mathcal{C}^{(i)}), \text{ then } \mathcal{C}_j^{(i)} \text{ is kept;} \quad (9)$$

otherwise $\mathcal{C}_j^{(i)}$ is removed, where $D(\mathcal{C}_j^{(i)}|\mathcal{C}^{(i)})$ is the average inter-distance from all samples in the sub-cluster $\mathcal{C}_j^{(i)}$ to other samples in cluster $\mathcal{C}^{(i)}$, and $D(\mathcal{C}^{(i)})$ is the average intra-distance among samples in cluster $\mathcal{C}^{(i)}$.

After such a post-processing step, the clusters of larger size are improved and at meantime, more singletons or tiny clusters are also produced. We denote the refined clusters as $\mathcal{C}' = \{\mathcal{C}^{(1)}, \mathcal{C}^{(2)}, \dots, \mathcal{C}^{(m')}\}$, where $m' \geq m$. Compared to tiny clusters and singletons, the larger clusters are more informative to provide pseudo supervision information to guide the contrastive learning.

Remark 2. In implementation, we use DBSCAN algorithm [3] to generate the raw clusters and to generate the over-segmentation of the clusters. DBSCAN [3] is a density-based clustering algorithm. It regards a data point as *density reachable* if the data point lies within a small distance threshold d to other samples, where the parameter d is the distance threshold to find neighboring point. Specifically, to generate the raw clusters, we employ DBSCAN with a slightly larger distance threshold parameter d (e.g., $d = 0.6$); whereas to generate the over-segmentation, we use a slightly smaller distance threshold parameter d' , where $d' := d - \delta$ (e.g., $\delta = 0.02$). We will show the influence of the parameters δ and d in experiments.

C. Training Procedure for Our CACL Approach

In CACL, the two branches in the siamese network are implemented with ResNet-50 [28] and they are not sharing parameters. We pre-train the two network branches on ImageNet at first and use the learned features to initialize the two memory banks \mathcal{M} and $\tilde{\mathcal{M}}$, respectively.

In training stage, we train both network branches at the same time with the total loss:

$$\mathcal{L} := \mathcal{L}_I + \mathcal{L}_C. \quad (10)$$

We update the two instance memory banks \mathcal{M} and $\tilde{\mathcal{M}}$, respectively, as follows:

$$\mathbf{v}_i^{(t)} \leftarrow \alpha \mathbf{v}_i^{(t-1)} + (1 - \alpha) \mathbf{x}_i, \quad (11)$$

$$\tilde{\mathbf{v}}_i^{(t)} \leftarrow \alpha \tilde{\mathbf{v}}_i^{(t-1)} + (1 - \alpha) \tilde{\mathbf{x}}_i, \quad (12)$$

where α is set as 0.2 by default (and we will discuss the influence of α in experiments).

In order to save the computation cost², we also use a stop-gradient operation as mentioned in SimSiam [9]. Note that we adopt the stop-gradient operation [9] to the second network branch $F'(\cdot|\Theta')$ when using the instance level loss \mathcal{L}_I in Eq. (1) to perform back propagation. Thus, the parameters Θ' in the second network branch are updated only with the intra-views cluster-level contrastive loss $\mathcal{L}_C^{(intra)}$ in Eq. (4).

Remark 3. For clarity, we summarize the details of the training procedure in Algorithm 1. We note that the “*asymmetry*” in the proposed framework for cluster-guided contrastive learning lies in following three aspects: a) asymmetry in network structure, i.e., a predictor layer is only added after the first branch³; and b) asymmetry in data augmentation, i.e., the augmented samples provided to the second branch are further transformed into gray-scale; c) asymmetry in pseudo labels generation, i.e., the output features of the first branch are used to generate pseudo labels which are shared with the second branch. Because of the asymmetry in the three aspects mentioned above, we term the proposed framework as Cluster-guided *Asymmetric* Contrastive Learning (CACL).

Remark 4. There have been many unsupervised Re-ID methods [17], [13], [29], [12] used the contrastive learning to learn discriminant features. Most of them [13], [29], [12] are Generative Adversarial Networks (GANs)-based methods and need additional supervised information to assist the training. For example, ATNet [13] trains multiple GANs through utilizing illumination and camera information, GCL [12] introduces the pose information in training, and AD-cluster [29] uses generating cross-camera samples to assist the training. Unlike these methods, our proposed CACL uses an asymmetric Siamese network to effectively learn fine-grained features by suppressing color with simple data augmentation operations during the training, rather than using an expensive sample generation via GANs. Compared to GANs based methods, our CACL is simple, efficient and effective.

D. Inference Procedure for CACL

After training, we keep only the ResNet $F(\cdot|\Theta)$ in the first branch for inference in testing.

To be specific, in the inference procedure, we use the output features \mathcal{X} of the first branch $F(\cdot|\Theta)$ to calculate the similarity between images. Given the query image dataset $\mathcal{I}^g = \{I_i^g\}_{i=1}^{N^g}$ and the gallery image dataset $\mathcal{I}^q = \{I_i^q\}_{i=1}^{N^q}$, where N^g and N^q are the sizes of the two datasets, respectively. For each image I_i^g in the query, we compute the distances between the query image and the images in the gallery \mathcal{I}^q via the feature

²Note that it is not necessary to use the stop-gradient operation in our CACL because the clustering result provides enough guide information under the asymmetric structure to prevent collapse. Although this is similar to the method in SimSiam [9], the purpose is different and it is not necessary to use in our proposal.

³It is also feasible to add another predictor layer after the second branch to have a symmetric network structure. Nevertheless, our experimental results show that merely marginal performance improvement can be yielded after adding an extra predictor layer. Thus, we prefer to use the asymmetric network architecture for the contrastive learning framework.

Algorithm 1 Training Procedure for CACL**Input:** Given a dataset $\mathcal{I} = \{I_i\}_{i=1}^N$.**Output:**

- 1: Pre-train the two network branches on ImageNet.
- 2: Initialize the two instance memory banks \mathcal{M} and $\tilde{\mathcal{M}}$ and set $P = P_{best} = 0$.
- 3: **while** epoch \leq total epoch **do**
- 4: Generate \hat{I}_i and \tilde{I}_i via data augmentation $\mathcal{T}(\cdot)$ and $\mathcal{G}(\mathcal{T}'(\cdot))$;
- 5: Perform feature extraction to get \mathbf{x}_i and $\tilde{\mathbf{x}}_i$;
- 6: Perform clustering and clustering refinement via Eq. (9) to yield pseudo label $\mathcal{Y} = \{\mathbf{y}_1, \dots, \mathbf{y}_N\}$;
- 7: Update the two cluster centers \mathcal{U} and $\tilde{\mathcal{U}}$ via Eq. (7);
- 8: Train siamese network, i.e., update Θ , Ψ and Θ' via the total loss in Eq. (10);
- 9: Update instance memory bank \mathcal{M} and $\tilde{\mathcal{M}}$ via Eq. (11) and Eq. (12);
- 10: Evaluate the model performance P with $F(\cdot|\Theta)$;
- 11: **if** $P > P_{best}$ **then**
- 12: Output the best model $F(\cdot|\Theta)$ and set $P_{best} \leftarrow P$;
- 13: **end if**
- 14: **end while**

obtained from the output of the first branch. And then, we sort the distance in ascending order to find the matched images.

IV. EXPERIMENTS

In this section, we describe the used benchmark datasets and the detailed parameter settings in experiments at first, and then provide extensive experiments on these datasets, including a set of detailed ablation study and a set of evaluation experiments to show the effect of each component. Finally, we give a set of data visualization experiments.⁴

A. Dataset Description

To evaluate the effectiveness of our proposal, we use the following three benchmark datasets: Market-1501 [41], DukeMTMC-ReID [45] and MSMT17 [46].

Market-1501 has 32,668 photos of 1501 people from six different camera views. The training set contains 12,936 of 751 identities. The testing set contains 19,732 images of 750 identities.

DukeMTMC-ReID consists of images sampling from DukeMTMC-ReID video dataset, 120 frames per video, with a total of 36,411 images of people of 1404 identities. The training set contains 16,522 images of 702 identities and the testing set contains 2228 query images of 702 identities and 17,661 gallery images. These images are taken from eight cameras.

MSMT17 has a total of 126,441 images under 15 camera views. The training set contains 32,621 images of 1041 identities. The testing set contains 93,820 images of 3060 identities are used for testing. MSMT17 is larger than Market-1501 and DukeMTMC-ReID.

⁴The code can be downloaded from <https://github.com/MingkunLishigure/CACL>.

B. Implementation Details

Settings for Training. In our CACL approach, we use ResNet-50 [28] pre-trained on ImageNet [11] for both network branches.⁵ The feature outputs $\mathbf{x}_i \in \mathbb{R}^D$ and $\tilde{\mathbf{x}}_i \in \mathbb{R}^D$ of the two networks $F(\cdot|\Theta)$ and $F(\cdot|\Theta')$ are D -dimensional vectors where $D = 2048$. We use the features output \mathbf{x}_i of the first branch $F(\cdot|\Theta)$ to perform clustering, where $\mathbf{x}_i = F(\hat{I}_i|\Theta) \in \mathbb{R}^D$.

The prediction layer $G(\cdot)$ is a $D \times D$ full connection layer. We initialize the two memory banks with the outputs of the feature from the corresponding network branches $F(\cdot|\Theta)$ and $F(\cdot|\Theta')$, respectively. We optimize the network through Adam optimizer [47] with a weight decay of 0.0005 and train the network with 80 epochs in total. The learning rate is initially set as 0.00035 and decreased to one-tenth per 20 epochs. The batch size is set to 64. The temperature coefficient τ in Eq. (6) is set to 0.05 and the update factor α in Eqs. (11) and (12) is set to 0.2.

Settings for Data Augmentation. In our experiments, we use the same data augmentation operations as other methods [17], [2], including random horizontal flip, random erasing and random crop, to define data augmentation $\mathcal{T}(\cdot)$ and $\mathcal{T}'(\cdot)$. Besides, we add a gray-scale transform to the input of the second branch.

Metrics for Performance Evaluation. In evaluation, we use the mean average precision (mAP) and cumulative matching characteristic (CMC) at Rank-1, 5, 10 to evaluate the performance.

C. Comparison to the State-of-the-art Methods

We compare our proposed CACL to the state-of-the-art unsupervised domain adaptation methods and purely unsupervised methods for person Re-ID. The purely unsupervised methods for person Re-ID include: CAMEL [40], PUL [19], SSL [20], LOMO [42], BOW [41], BUC [18], HCT [4], SpCL [17], and CAP [43]. The unsupervised domain adaptation methods for person Re-ID include: PTGAN [30], ADTC [36], HHL [35], SSG [5], MMCL [23], AD-Cluster [29], MEB [38], NRMT [39], SPGAN [32], TJ-AIDL [16], JVTC [37], PGPPM [34], and MMT [2].

The comparison results of the state-of-the-art unsupervised domain adaptation methods and purely unsupervised methods are shown in Table I. We can find that our proposed CACL achieves 80.9/92.7% at mAP/Rank-1 on Market-1501 and 69.6/82.6% at mAP/Rank-1 on DukeMTMC-ReID, respectively. It can be found that CACL not only performs better than all pure unsupervised methods but also achieves the best performance than unsupervised domain adaptation methods.

Moreover, we also conduct experiments on a much larger dataset MSMT17 and report the experimental results in Table II. Again, we can observe that our proposed CACL achieves a leading performance, i.e., 23.0/48.4% at mAP/Rank-1. It is worth to note that our CACL yields superior performance than some UDA methods on this challenging dataset. These results confirm the effectiveness of our proposal.

⁵In Section IV-C, we also provide the performance evaluation with other backbone networks for the two branches.

TABLE I

COMPARISON TO OTHER STATE-OF-THE-ART METHODS. 'UDA' IS TO REFER THE UNSUPERVISED DOMAIN ADAPTATION METHODS AND 'US' IS TO REFER THE PURELY UNSUPERVISED LEARNING METHODS. '*' MEANS THAT THE USED BACKBONE IS PRE-TRAINED ON IMAGENET.

Method	Type	Reference	Bakcbone	Market-1501				DukeMTMC-ReID			
				mAP	Rank-1	Rank-5	Rank-10	mAP	Rank-1	Rank-5	Rank-10
PTGAN [30]	UDA	CVPR'18	GoogleNet [31]	15.7	38.6	57.3	-	13.5	27.4	43.6	-
SPGAN [32]	UDA	CVPR'18	ResNet50* [28]	26.7	58.1	76.0	82.7	26.4	46.9	62.6	68.5
TJ-AIDL [16]	UDA	CVPR'18	MobileNet* [33]	26.5	58.2	74.8	-	23.0	44.3	59.6	-
PGPPM [34]	UDA	CVPR'18	ResNet50* [28]	33.9	63.9	81.1	86.4	17.9	36.3	54.0	61.6
HHL [35]	UDA	ECCV'18	ResNet50* [28]	31.4	62.2	78.0	84.0	27.2	46.9	61.0	66.7
SSG [5]	UDA	ECCV'19	ResNet50* [28]	58.3	80.0	90.0	92.4	53.4	73.0	80.6	83.2
AD-cluster [29]	UDA	CVPR'20	ResNet50* [28]	68.3	86.7	94.4	96.5	54.1	72.6	82.5	85.5
ADTC [36]	UDA	ECCV'20	ResNet50* [28]	59.7	79.3	90.8	94.1	52.5	71.9	84.1	87.5
MMCL [23]	UDA	CVPR'20	ResNet50* [28]	60.4	84.4	92.8	95.0	51.4	72.4	82.9	85.0
MMT [2]	UDA	ICLR'20	ResNet50* [28]	73.8	89.5	96.0	97.6	62.3	76.3	87.7	91.2
JVTC [37]	UDA	ECCV'20	ResNet50* [28]	67.2	86.8	95.2	97.1	66.5	80.4	89.9	93.7
MEB [38]	UDA	ECCV'20	ResNet50* [28]	76.0	89.9	95.2	96.9	65.3	81.2	90.9	92.2
NRMT [39]	UDA	ECCV'20	ResNet50* [28]	71.7	87.8	94.6	96.5	62.2	77.8	86.9	89.5
SpCL [17]	UDA	NIPS'20	ResNet50* [28]	76.7	90.3	96.2	97.7	68.8	82.9	90.1	92.5
CAMEL [40]	US	ICCV'17	ResNet50* [28]	26.3	54.4	73.1	79.6	19.8	40.2	57.5	64.9
Bow [41]	US	ICCV'15	-	14.8	35.8	52.4	60.3	8.5	17.1	28.8	34.9
PUL [19]	US	TOMM'18	ResNet50* [28]	22.8	51.5	70.1	76.8	22.3	41.1	46.6	63.0
LOMO [42]	US	CVPR'15	-	8.0	27.2	41.6	49.1	4.8	12.3	21.3	26.6
BUC [18]	US	AAAI'19	ResNet50* [28]	30.6	61.0	71.6	76.4	21.9	40.2	52.7	57.4
HCT [4]	US	CVPR'20	ResNet50* [28]	56.4	80.0	91.6	95.2	50.1	69.6	83.4	87.4
SSL [20]	US	CVPR'20	ResNet50* [28]	37.8	71.7	83.8	87.4	28.6	52.5	63.5	68.9
SpCL [17]	US	NIPS'20	ResNet50* [28]	73.1	88.1	96.3	97.7	65.3	81.2	90.3	92.2
CAP [43]	US	AAAI'20	ResNet50* [28]	79.2	91.4	96.3	97.7	67.3	81.1	89.3	91.8
CACL	US	This paper	ResNet50* [28]	80.9	92.7	97.4	98.5	69.6	82.6	91.2	93.8
CACL	US	This paper	IBN-ResNet* [44]	83.6	93.3	97.7	98.3	72.5	85.5	92.9	94.9

TABLE II
EXPERIMENTAL RESULTS ON MSMT17.

Method	Type	Reference	MSMT17			
			mAP	Rank-1	Rank-5	Rank-10
PTGAN [30]	UDA	CVPR'18	3.3	11.8	-	27.4
ECN [48]	UDA	CVPR'19	10.2	30.2	41.5	46.8
SSG [5]	UDA	ICCV'19	13.3	32.2	-	51.2
MMCL [23]	UDA	CVPR'20	16.2	43.6	54.3	58.9
JVTC+ [37]	US	ECCV'20	17.3	43.1	53.8	59.4
SpCL [17]	US	NIPS'20	19.1	42.3	55.6	61.2
MMT [2]	UDA	ICLR'20	24.0	50.1	63.5	69.3
SpCL [17]	UDA	NIPS'20	26.8	53.7	79.3	83.1
CACL	US	This paper	23.0	48.9	61.2	66.4
CACL w/ IBN-ResNet	US	This paper	29.9	57.1	68.4	73.1

Note that Instance-Batch Normalization (IBN) [44] has been used in object recognition and has been proved very effective. Here, we evaluate our CACL, in which the backbone is implemented with Instance-Batch Normalization ResNet (IBN-ResNet). Similar to CACL with ResNet [28], we introduce an Instance-Batch Normalization (IBN) layer to replace the BN layer and call it an IBN-ResNet. As shown in Table I, the performance of our CACL can be further improved when combining with IBN-ResNet.

D. Ablation Study

To evaluate the effectiveness of each component: \mathcal{L}_I , $\mathcal{L}_C^{(inter)}$, $\mathcal{L}_C^{(intra)}$ and clustering with refinement in our CACL approach, we conduct a set of ablation experiments on Market-1501 and DukeMTMC-ReID.

In the baseline method, we train both branches with data augmentation $\mathcal{T}'(\cdot)$ and $\mathcal{T}(\cdot)$ by using the Non-Parametric Softmax loss [49], which is defined as

$$\mathcal{L}(\mathbf{x}_i) = -\ln\left(\frac{\exp(\mathbf{u}_{\omega(I_i)}^\top \mathbf{x}_i / \tau)}{\sum_{\ell=1}^{m'} \exp(\mathbf{u}_\ell^\top \mathbf{x}_i / \tau)}\right), \quad (13)$$

and both the training process and the memory updating strategy in the baseline method are kept the same as our CACL method.

To comprehensively evaluate the contribution of each component, we conduct a set of ablation experiments by testing each component in our CACL framework individually, i.e., cluster refinement, instance-level contrastive loss \mathcal{L}_I and cluster-level contrastive loss \mathcal{L}_C . To further evaluate the sub-part of the cluster-level contrastive loss, we also conduct experiments to evaluate the influence of using $\mathcal{L}_C^{(inter)}$ or $\mathcal{L}_C^{(intra)}$, separately.

In the ablation experiments, to test the model with contrastive loss \mathcal{L}_C or \mathcal{L}_I , we train both branches with data augmentation $\mathcal{T}'(\cdot)$ and $\mathcal{G}(\mathcal{T}'(\cdot))$, respectively. To test the model performance with the cluster-level contrastive loss \mathcal{L}_C and the sub-part of $\mathcal{L}_C^{(intra)}$, compared to the baseline method, we need to replace the Non-Parametric Softmax loss in Eq. (13) by the loss in Eq. (4) for both branches. The results of the ablation study are reported in Table III.

As can be read in Table III, the performance improves when each component is used individually. This validates that each component contributes to the performance improvements. For the experiments of using both \mathcal{L}_C and \mathcal{L}_I , it does not significantly better than just using \mathcal{L}_I , and in the experiments of using \mathcal{L}_C we observe a slight improvement than the baseline.

TABLE III
ABLATION STUDY ON MARKET-1501 AND DUKEMTMC-REID.

Components	Cluster Refine	\mathcal{L}_I	\mathcal{L}_C^{intra}	\mathcal{L}_C^{inter}	Market-1501				DukeMTMC-ReID			
					mAP	Rank-1	Rank-5	Rank-10	mAP	Rank-1	Rank-5	Rank-10
Baseline					68.1	85.2	94.0	96.0	62.5	78.5	88.5	90.3
+ \mathcal{L}_C			✓	✓	70.8	87.5	94.4	96	62.5	79.5	88.4	90.8
+ \mathcal{L}_I		✓			74.7	88.7	95	96.6	64.2	80.7	89	91.6
+ $\mathcal{L}_I + \mathcal{L}_C$		✓	✓	✓	74.4	89.3	95.9	96.7	63.8	79.2	89.2	91.7
+ Cluster Refine	✓				73	87.8	95.7	97.2	65.7	81.1	90.6	93.2
+ Cluster Refine + \mathcal{L}_I	✓	✓			78.2	91.2	97	98.1	67.6	81.8	90.2	93
+ Cluster Refine + $\mathcal{L}_I + \mathcal{L}_C^{inter}$	✓	✓		✓	78.7	91.2	97	97.9	68.5	81.9	91.2	93.8
+ Cluster Refine + $\mathcal{L}_I + \mathcal{L}_C^{intra}$	✓	✓	✓		79.2	91.9	96.7	98	68.3	82.1	90.3	93.2
+ Cluster Refine + \mathcal{L}_C	✓		✓	✓	80.4	92.2	97.1	98.2	68.8	82.2	91.3	93.8
Our CACL	✓	✓	✓	✓	80.9	92.7	97.4	98.5	69.6	82.6	91.2	93.8

This is because the clustering result is not high quality and using \mathcal{L}_C will make the training pay more attention to the noisy cluster information. Therefore, it might bring misleading information to the network training. In the experiments of using both \mathcal{L}_C and cluster refinement, we observe significant performance improvement than using the cluster refinement alone. This also validates that the cluster refinement improves the clustering result and the refined clustering information can further enhance the effectiveness of using \mathcal{L}_C to train the network.

E. More Evaluation and Analysis

Evaluation on Importance of Cluster-Guided. We use an instance-level contrastive loss in our method to mine the invariance between different augment views based on SimSiam [9]. To verify whether the clustering guidance is vital in the contrast learning framework, we train our CACL framework but just using the instance-level contrastive loss in Eq. (1) without the clustering guidance. The experimental results are shown in Table IV. As can be read from Table IV, surprisingly, the contrastive learning framework without clustering guidance did not work at all.

TABLE IV
ABLATION STUDY ON MARKET-1501.

Components	Market-1501			
	mAP	Rank-1	Rank-5	Rank-10
CACL w/o clustering	0.3	0.5	1.2	2.3
CACL w/o <i>stopGrad</i>	80.2	92.0	97.0	97.6
CACL	80.9	92.7	97.4	98.5

Improvements Brought by Suppressing Colors. To suppress colors influence, CACL uses a gray-scale process $\mathcal{G}(\cdot)$ over the data augmentation $\mathcal{T}'(\cdot)$ for the second network branch. To validate the effectiveness of suppressing colors, we conduct a set of experiments under different settings: a) simply using data augmentation $\mathcal{T}'(\cdot)$ with raw color; b) using another data augmentation approach, named “color-jitter”, which denoted as $\mathcal{J}(\cdot)$ to replace $\mathcal{G}(\cdot)$, which output is still a color image; c) with gray-scale transform $\mathcal{G}(\cdot)$ after $\mathcal{T}'(\cdot)$. It should be emphasized that in the implementation, the “color-jitter” operation will give random amplitude values to the image changing. We display the image samples processed with different data



Fig. 4. Illustration for the raw images and the augmented images. The 1st row: “raw images”. The 2nd row: “color-jitter”. Bottom row: “gray-scale”.

TABLE V
PERFORMANCE COMPARISON ON USING COLOR DATA AUGMENTATIONS AND GRAY-SCALE TRANSFORM TO THE SECOND NETWORK BRANCH.

Components	Cluster Refine	Market-1501			
		mAP	Rank-1	Rank-5	Rank-10
$\mathcal{T}'(\cdot)$		70.3	87.4	94.6	96.5
$\mathcal{J}(\mathcal{T}'(\cdot))$		72.5	87.8	95.3	96.9
$\mathcal{G}(\mathcal{T}'(\cdot))$		74.4	89.3	95.9	96.7
$\mathcal{T}'(\cdot)$	✓	79.0	90.6	96.3	97.1
$\mathcal{J}(\mathcal{T}'(\cdot))$	✓	79.1	90.8	96.7	97.8
$\mathcal{G}(\mathcal{T}'(\cdot))$	✓	80.9	92.7	97.4	98.5

augmentation methods in Fig. 4. As can be observed, “color-jitter” did change the image, but the color information still dominates.

Experimental results are provided in Table V. We can read that using “color-jitter” $\mathcal{J}(\cdot)$ yields some performance improvement, but using “gray-scale” $\mathcal{G}(\cdot)$ yield the best performance improvement. When combined with the cluster refinement step, we can observe the similar result that: using “gray-scale” $\mathcal{G}(\cdot)$ yields better performance improvement than using “color-jitter” $\mathcal{J}(\cdot)$. These results validate that suppressing colors is effective to gain performance improvement. Compared to using “gray-scale”, using “color-jitter” does not truly eliminate the influence brought by colors, that is to say, after using color-jitter, the color information still dominates.

To further reveal the mechanisms why using “gray-scale” works better than using “color-jitter” in the proposed framework, we show the statistic histograms of color distributions

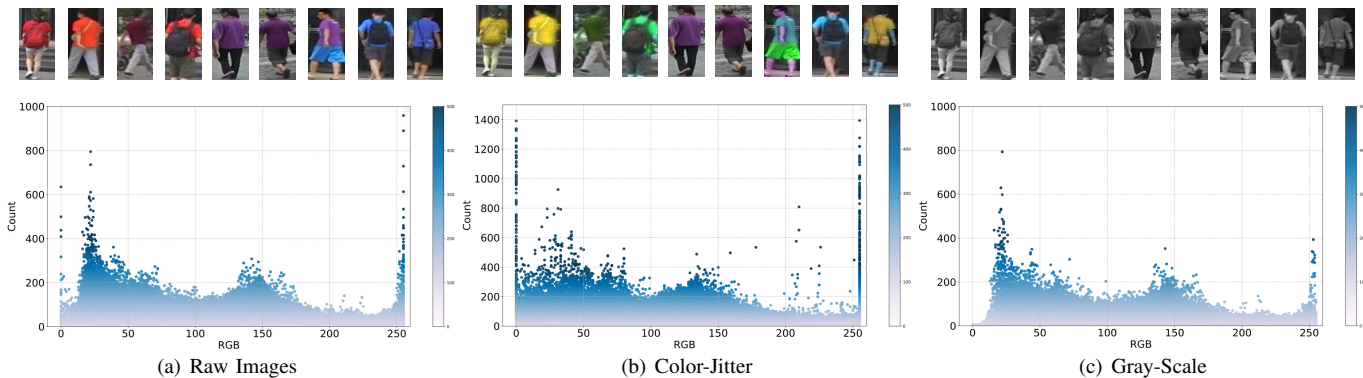


Fig. 5. Comparison on distributions in histogram of intensity in RGB channels under different data augmentation operations.

of using raw image, color-jitter, and gray-scale, respectively. Specifically, we compute the statistical histograms of the intensity values in the RGB channels of the raw color images and the images after using “color-jitter” and “gray-scale” with 500 images sampled at random in the training data from Market-1501. The statistical results are shown in Fig. 5.

We can observe that: using “gray-scale” yields roughly consistent distribution in the histogram compared to the raw images; whereas using the distribution in the histogram of the images after using “color-jitter” has some notable deviations from that of the raw images. In the histogram of using “gray-scale”, the proportion of the pixels at the two extreme values (i.e., 0 and 255) are significantly reduced; whereas in the histogram of using “color-jitter”, the proportion of the pixels at the two extreme values, especially at 0, are significantly magnified—this phenomenon might damage the content consistency with the raw image. The difference in the consistency of the histogram reveals the essential advantage of using “gray-scale” to suppress the influence of colors, rather than using “color-jitter”.

Evaluation on Parameters in DBSCAN. We conduct experiments evaluate the parameter d to find the neighbors. In cluster refinement, we use DBSCAN with a smaller parameter d' , where $d' := d - \delta$ to find the over-segmentation. We conduct experiments on Market-1501 to evaluate the effects of changing the two parameters. Experiments are recorded in Table VI. we can find that while the change of d will affect the baseline performance, our CACL still improves the model performance significantly. Note that even though the baseline performance will sharply drop when using $d = 0.7$, our method can also achieve a good performance which is also higher than other unsupervised methods in Table I.

The cluster refinement is an important component in our proposed CACL, and δ is an important parameter to find the over-segmentation of the raw clusters. Thus, we further conduct experiments to evaluate the performance of using different values of δ . Experimental results are shown in Table VII. We can find that the performance is not too sensitive to δ . When using $\delta = 0.02$, the performance achieves the best, i.e., 80.9/92.7% at mAP/Rank-1 on Market-1501 and 69.6/82.6% at mAP/Rank-1 on DukeMTMC-ReID.

Moreover, we also test the stop-gradient operations under

TABLE VI
PERFORMANCE COMPARISON OF DIFFERENT CLUSTER PARAMETER d (THE MAXIMUM DISTANCE BETWEEN NEIGHBOR POINTS) ON CACL AND BASELINE METHOD.

d	Market-1501				DukeMTMC-ReID			
	Baseline		CACL		Baseline		CACL	
	mAP	Rank-1	mAP	Rank-1	mAP	Rank-1	mAP	Rank-1
0.4	68.6	85.9	75.2	91.4	60.1	77.5	62.0	77.7
0.5	71.2	86.5	81.6	93.0	63.4	80.3	67.5	81.8
0.6	68.1	85.2	80.9	92.7	62.5	78.5	69.6	82.6
0.7	43.8	71.5	75.8	90.1	4.1	10.3	66.7	80.6

TABLE VII
ILLUSTRATION FOR THE MODEL PERFORMANCE WITH DIFFERENT δ ON MARKET-1501.

δ	Market-1501							
	$d = 0.4$		$d = 0.5$		$d = 0.6$		$d = 0.7$	
	mAP	Rank-1	mAP	Rank-1	mAP	Rank-1	mAP	Rank-1
0.02	75.2	91.4	81.6	93.0	80.9	92.7	75.8	90.1
0.04	70.8	89.5	80.4	92.6	80.3	92.3	68.7	86.2
0.06	65.8	87.2	77.7	91.7	79.0	91.4	8.20	20.3
0.08	64.3	86.2	76.6	91.2	78.5	91.3	6.10	15.6

different structures. In Table IV, as can be read that, the performance of the framework with asymmetric structure drops slightly (i.e., only 0.7% lower than that of using the stop-gradient operation) when the stop-gradient operation is not used. This hints that the framework with asymmetric structure in CACL does not highly depend on the stop-gradient operation.

Evaluation Performance of Two Branches. To further reveal the performance of the trained networks, we record the performance of using the output features of each branch of two networks $F(\cdot|\Theta)$ and $F'(\cdot|\Theta')$, separately, for person ReID in Table VIII. We can read that using the output features of the second branch $F'(\cdot|\Theta')$ did yield significantly lower performance than that of using the output feature of the first branch $F(\cdot|\Theta)$, and the result of using $F'(\cdot|\Theta')$ is similar to the result of the experiments without using $\mathcal{L}_C^{(intra)}$. This is because the second network branch pays attention to learning features from gray-scale images, lacking of the ability to capture richer information from color images.

Evaluation on Memory Update Parameter α . We conduct

TABLE VIII
PERFORMANCE COMPARISON ON $F(\cdot|\Theta)$ AND $F'(\cdot|\Theta')$.

Branch	Market-1501			
	mAP	Rank-1	Rank-5	Rank-10
$F(\cdot \Theta)$ (Color)	80.9	92.7	97.4	98.5
$F'(\cdot \Theta')$ (Gray-Scale)	43.8	71.5	83.9	87.1

TABLE IX
PERFORMANCE COMPARISON ON DIFFERENT α .

Branch	Market-1501			
	mAP	Rank-1	Rank-5	Rank-10
0.0	75.1	89.8	96.3	97.3
0.2	80.9	92.7	97.4	98.5
0.4	80.8	92.5	97.1	98.2
0.6	80.2	92.4	97.2	98.3
0.8	77.3	90.9	96.6	98.0
1.0	4.3	10.9	19.9	24.9

experiments to evaluate the effects of the memory update parameter α and show the results in Table IX. We can find that our CACL is not sensitive to the changing of memory update parameter α , except for $\alpha = 1$. When using $\alpha = 1$, the model performance significantly drops because the memory bank has not been updated at this time. When using $\alpha = 0.2$ the model achieves the best performance on Market-1501, i.e., 80.9/92.7% at mAP/Rank-1.

Evaluation on Performance with Ground-truth Labels. We compare our CACL to the baseline method with the ground-truth labels (i.e., in supervised setting). The results are shown in Table X. We can find that CACL could achieve good performance under unsupervised setting, which is merely lower 3/1.1% at mAP/Rank-1 than the baseline method, which is trained with the ground-truth labels on Market-1501. Moreover, if we provide ground-truth labels to train our CACL (i.e., CACL+labels), notable improvements in performance than the supervised baseline method can be observed.

F. Data Visualization

To gain some intuitive understanding of the performance of our proposed CACL, we conduct a set of data visualization experiments on Market-1501 to visualize the clustering results of the learned features when different training strategies are used: a) without using the contrastive loss $\mathcal{L}_C + \mathcal{L}_I$; and b) using the contrastive losses $\mathcal{L}_C + \mathcal{L}_I$.

TABLE X
PERFORMANCE COMPARISON TO BASELINE METHOD IN SUPERVISED SETTING. "BASELINE + LABELS" MEANS THAT WE USE THE GROUND-TRUTH LABELS TO TRAIN THE BASELINE METHOD; WHEREAS "CACL + LABELS" MEANS THAT WE USE THE GROUND-TRUTH LABELS TO TRAIN OUR CACL.

Method	Market-1501		DukeMTMC-ReID	
	mAP	Rank-1	mAP	Rank-1
CACL	80.9	92.7	69.6	82.6
Baseline + labels	83.9	93.6	73.3	86.6
CACL + labels	85.7	94.2	74.9	87.2

Experimental results are shown in Fig. 6. We can observe that the contrastive loss $\mathcal{L}_C + \mathcal{L}_I$ did help the model distinguish those similar images while maintaining the cluster compactness, and also separate the overlapping individual samples from each other. This confirms the effectiveness of our proposed approach, and it also shows that our approach can attenuate the influence of clothing color.

At the same time, we also selected some query samples with the top-10 best matching images in the gallery set and show them in Fig. 7. Compared to the baseline model, our approach returns more accurate results. We can find that most of the wrong samples matched by the baseline model are dressed in the same color with the query sample. These results suggest that our approach can effectively ignore the interference caused by samples with similar colors and thus find more accurate matches.

V. CONCLUSION

We have proposed a Cluster-guided Asymmetric Contrastive Learning (CACL) approach for unsupervised person Re-ID, in which cluster information is leveraged to guide the feature learning in a properly designed contrastive learning framework. Specifically, in our proposed CACL, instance-level contrastive learning is conducted with respect to the asymmetric data augmentation and cluster-level contrastive learning is conducted with respect to the refined clustering result. By leveraging the refined cluster result into contrastive learning, CACL is able to effectively exploit the invariance within and between different data augmentation views for learning more effective features beyond the dominating colors. In addition, we confirmed that refined clustering result could help our CACL approach mine invariant information more effectively at the cluster level. We have conducted extensive experiments on three benchmark datasets and demonstrated the superior performance of our proposal.

As the future work, it is interesting and promising to incorporate attention mechanism (e.g., [50], [51]), clustering ensemble and hybrid contrastive learning strategy (e.g., [52]) or side information in dataset (e.g., [12]) to further enrich the representation capacity, improve the stability and enhance the overall performance of the proposed framework. What's more, in other related fields, such as face recognition or vehicle re identification (e.g., [53], [54]), whether suppresses the dominating color can also bring positive influence is a very interesting and worth exploring direction.

REFERENCES

- [1] L. Zheng, Y. Yang, and A. G. Hauptmann, "Person re-identification: Past, present and future," *arXiv preprint arXiv:1610.02984*, 2016. **1, 2**
- [2] Y. Ge, D. Chen, and H. Li, "Mutual mean-teaching: Pseudo label refinery for unsupervised domain adaptation on person re-identification," in *International Conference on Learning Representations*, 2020. **1, 6, 7**
- [3] M. Ester, H.-P. Kriegel, J. Sander, and X. Xu, "A density-based algorithm for discovering clusters in large spatial databases with noise," in *Second International Conference on Knowledge Discovery and Data Mining*, 1996, p. 226–231. **1, 5**
- [4] K. Zeng, M. Ning, Y. Wang, and Y. Guo, "Hierarchical clustering with hard-batch triplet loss for person re-identification," in *IEEE Conference on Computer Vision and Pattern Recognition*, 2020, pp. 13 657–13 665. **1, 2, 6, 7**

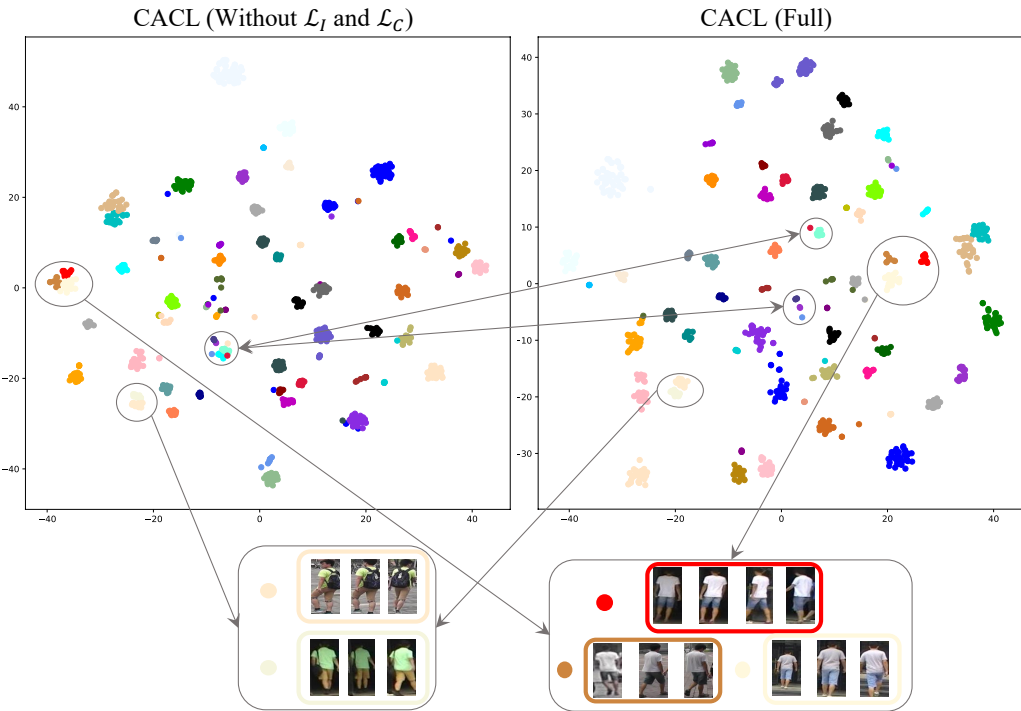


Fig. 6. Data Visualization via t -SNE of the learned feature and clusters under two different training strategies: Training without \mathcal{L}_C and \mathcal{L}_I (left) as mentioned in Table III and our CACL (right). The data points come from the Market-1501 training set (1,000 images of 60 identities). The points with the same color mean the image of the same identity. To demonstrate the difference between the two distributions in detail, we further zoom in on the circled clusters and show the corresponding images. The images in the boxes are similar to each other and the corresponding data points are very close to each other or even overlapping in the feature space if the model is trained without using \mathcal{L}_C and \mathcal{L}_I , as shown in the left box; whereas using the contrastive losses \mathcal{L}_C and \mathcal{L}_I will effectively distinguish these data points and maintain the cluster compactness as shown in the right box.

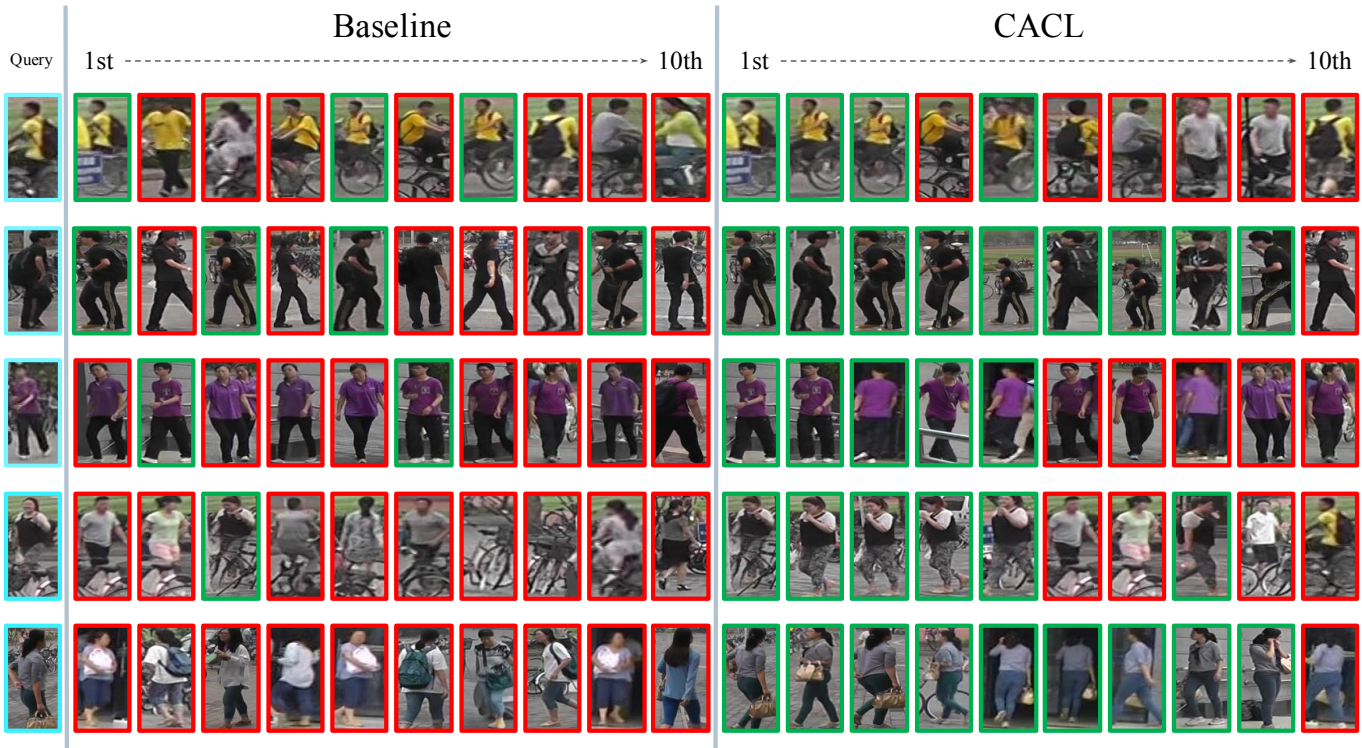


Fig. 7. Visualization of the top-10 best matched images. We show the top-10 best matching samples in the gallery set for the query sample with the baseline method and our proposed CACL. The images with frames in green and in red are the correctly matched images and mismatched images, respectively.

- [5] Y. Fu, Y. Wei, G. Wang, Y. Zhou, H. Shi, and T. S. Huang, "Self-similarity grouping: A simple unsupervised cross domain adaptation approach for person re-identification," in *The IEEE International Conference on Computer Vision*, October 2019, pp. 6112–6121. **1, 6, 7**
- [6] J. Xie, X. Zhan, Z. Liu, Y. S. Ong, and C. C. Loy, "Delving into inter-image invariance for unsupervised visual representations," in *Conference and Workshop on Neural Information Processing Systems*, 2020. **1, 3**
- [7] M. Caron, I. Misra, J. Mairal, P. Goyal, P. Bojanowski, and A. Joulin, "Unsupervised learning of visual features by contrasting cluster assignments," *Advances in Neural Information Processing Systems*, pp. 9912–9924, 2020. **1, 3**
- [8] T. Chen, S. Kornblith, M. Norouzi, and G. Hinton, "A simple framework for contrastive learning of visual representations," in *International Conference on Machine Learning*, 2020, pp. 1597–1607. **1, 3, 4**
- [9] X. Chen and K. He, "Exploring simple siamese representation learning," in *IEEE Conference on Computer Vision and Pattern Recognition*, 2021, pp. 15 750–15 758. **1, 3, 5, 8**
- [10] J.-B. Grill, F. Strub, F. Alché, C. Tallec, P. Richemond, E. Buchatskaya, C. Doersch, B. Avila Pires, Z. Guo, M. Gheshlaghi Azar, B. Piot, k. kavukcuoglu, R. Munos, and M. Valko, "Bootstrap your own latent - a new approach to self-supervised learning," in *Advances in Neural Information Processing Systems*, 2020, pp. 21 271–21 284. **1, 3, 4**
- [11] A. Krizhevsky, I. Sutskever, and G. E. Hinton, "Imagenet classification with deep convolutional neural networks," in *Conference and Workshop on Neural Information Processing Systems*, 2012, pp. 1097–1105. **1, 4, 6**
- [12] H. Chen, Y. Wang, B. Lagadeç, A. Dantcheva, and F. Bremond, "Joint generative and contrastive learning for unsupervised person re-identification," in *IEEE Conference on Computer Vision and Pattern Recognition*, June 2021, pp. 2004–2013. **2, 5, 10**
- [13] J. Liu, Z.-J. Zha, D. Chen, R. Hong, and M. Wang, "Adaptive transfer network for cross-domain person re-identification," in *IEEE Conference on Computer Vision and Pattern Recognition*, 2019, pp. 7202–7211. **2, 5**
- [14] S. Bak, P. Carr, and J.-F. Lalonde, "Domain adaptation through synthesis for unsupervised person re-identification," in *European Conference on Computer Vision*, 2018, pp. 189–205. **2**
- [15] P. Peng, T. Xiang, Y. Wang, M. Pontil, S. Gong, T. Huang, and Y. Tian, "Unsupervised cross-dataset transfer learning for person re-identification," in *IEEE Conference on Computer Vision and Pattern Recognition*, 2016, pp. 1306–1315. **2**
- [16] J. Wang, X. Zhu, S. Gong, and W. Li, "Transferable joint attribute-identity deep learning for unsupervised person re-identification," in *IEEE Conference on Computer Vision and Pattern Recognition*, 2018, pp. 2275–2284. **2, 6, 7**
- [17] Y. Ge, F. Zhu, D. Chen, R. Zhao, and H. Li, "Self-paced contrastive learning with hybrid memory for domain adaptive object re-id," in *Advances in Neural Information Processing Systems*, 2020, pp. 11 309–11 321. **2, 5, 6, 7**
- [18] Y. Lin, X. Dong, L. Zheng, Y. Yan, and Y. Yang, "A bottom-up clustering approach to unsupervised person re-identification," in *The Association for the Advancement of Artificial Intelligence*, vol. 33, 2019, pp. 8738–8745. **2, 6, 7**
- [19] H. Fan, L. Zheng, C. Yan, and Y. Yang, "Unsupervised person re-identification: Clustering and fine-tuning," *ACM Transactions on Multimedia Computing, Communications, and Applications*, vol. 14, no. 4, p. 83, 2018. **2, 6, 7**
- [20] Y. Lin, L. Xie, Y. Wu, C. Yan, and Q. Tian, "Unsupervised person re-identification via softened similarity learning," in *IEEE Conference on Computer Vision and Pattern Recognition*, 2020, pp. 3390–3399. **2, 6, 7**
- [21] B. Sun, J. Feng, and K. Saenko, "Return of frustratingly easy domain adaptation," in *Association for the Advancement of Artificial Intelligence*, vol. 30, 2016. **2**
- [22] Y. Ganin and V. Lempitsky, "Unsupervised domain adaptation by backpropagation," in *International Conference on Machine Learning*, 2015, pp. 1180–1189. **2**
- [23] D. Wang and S. Zhang, "Unsupervised person re-identification via multi-label classification," in *IEEE Conference on Computer Vision and Pattern Recognition*, 2020, pp. 10 981–10 990. **2, 6, 7**
- [24] P. Bojanowski and A. Joulin, "Unsupervised learning by predicting noise," in *International Conference on Machine Learning*. PMLR, 2017, pp. 517–526. **3**
- [25] A. Dosovitskiy, P. Fischer, J. T. Springenberg, M. Riedmiller, and T. Brox, "Discriminative unsupervised feature learning with exemplar convolutional neural networks," *IEEE Transactions on Pattern Analysis and Machine Intelligence*, vol. 38, no. 9, pp. 1734–1747, 2015. **3**
- [26] Y. Li, P. Hu, Z. Liu, D. Peng, J. T. Zhou, and X. Peng, "Contrastive clustering," in *AAAI Conference on Artificial Intelligence*, 2021. **3**
- [27] K. He, H. Fan, Y. Wu, S. Xie, and R. Girshick, "Momentum contrast for unsupervised visual representation learning," in *IEEE Conference on Computer Vision and Pattern Recognition*, 2020, pp. 9729–9738. **3**
- [28] K. He, X. Zhang, S. Ren, and J. Sun, "Deep residual learning for image recognition," in *IEEE Conference on Computer Vision and Pattern Recognition*, 2016, pp. 770–778. **3, 5, 6, 7**
- [29] Y. Zhai, S. Lu, Q. Ye, X. Shan, J. Chen, R. Ji, and Y. Tian, "Ad-cluster: Augmented discriminative clustering for domain adaptive person re-identification," in *IEEE Conference on Computer Vision and Pattern Recognition*, 2020, pp. 9021–9030. **5, 6, 7**
- [30] L. Wei, S. Zhang, W. Gao, and Q. Tian, "Person transfer gan to bridge domain gap for person re-identification," in *IEEE Conference on Computer Vision and Pattern Recognition*, 2018, pp. 79–88. **6, 7**
- [31] C. Szegedy, W. Liu, Y. Jia, P. Sermanet, S. Reed, D. Anguelov, D. Erhan, V. Vanhoucke, and A. Rabinovich, "Going deeper with convolutions," in *IEEE Conference on Computer Vision and Pattern Recognition*, 2015, pp. 1–9. **7**
- [32] W. Deng, L. Zheng, Q. Ye, G. Kang, Y. Yang, and J. Jiao, "Image-image domain adaptation with preserved self-similarity and domain-dissimilarity for person re-identification," in *IEEE Conference on Computer Vision and Pattern Recognition*, 2018, pp. 994–1003. **6, 7**
- [33] A. G. Howard, M. Zhu, B. Chen, D. Kalenichenko, W. Wang, T. Weyand, M. Andreetto, and H. Adam, "Mobilenets: Efficient convolutional neural networks for mobile vision applications," *arXiv preprint arXiv:1704.04861*, 2017. **7**
- [34] F. Yang, Z. Zhong, Z. Luo, S. Lian, and S. Li, "Leveraging virtual and real person for unsupervised person re-identification," *IEEE Transactions on Multimedia*, vol. 22, no. 9, pp. 2444–2453, 2019. **6, 7**
- [35] Z. Zhong, L. Zheng, S. Li, and Y. Yang, "Generalizing a person retrieval model hetero-and homogeneously," in *European Conference on Computer Vision*, 2018, pp. 172–188. **6, 7**
- [36] Z. Ji, X. Zou, X. Lin, X. Liu, T. Huang, and S. Wu, "An attention-driven two-stage clustering method for unsupervised person re-identification," in *European Conference on Computer Vision*, 2020, pp. 20–36. **6, 7**
- [37] J. Li and S. Zhang, "Joint visual and temporal consistency for unsupervised domain adaptive person re-identification," in *European Conference on Computer Vision*, 2020. **6, 7**
- [38] Y. Zhai, Q. Ye, S. Lu, M. Jia, R. Ji, and Y. Tian, "Multiple expert brainstorming for domain adaptive person re-identification," in *European Conference on Computer Vision*, 2020, pp. 594–611. **6, 7**
- [39] F. Zhao, S. Liao, G.-S. Xie, J. Zhao, K. Zhang, and L. Shao, "Unsupervised domain adaptation with noise resistible mutual-training for person re-identification," in *European Conference on Computer Vision*. Springer, 2020, pp. 526–544. **6, 7**
- [40] H.-X. Yu, A. Wu, and W.-S. Zheng, "Cross-view asymmetric metric learning for unsupervised person re-identification," in *IEEE International Conference on Computer Vision*, 2017, pp. 994–1002. **6, 7**
- [41] L. Zheng, L. Shen, L. Tian, S. Wang, J. Wang, and Q. Tian, "Scalable person re-identification: A benchmark," in *IEEE International Conference on Computer Vision*, 2015, pp. 1116–1124. **6, 7**
- [42] S. Liao, Y. Hu, X. Zhu, and S. Z. Li, "Person re-identification by local maximal occurrence representation and metric learning," in *IEEE Conference on Computer Vision and Pattern Recognition*, 2015, pp. 2197–2206. **6, 7**
- [43] M. Wang, B. Lai, J. Huang, X. Gong, and X.-S. Hua, "Camera-aware proxies for unsupervised person re-identification," in *AAAI Conference on Artificial Intelligence*, vol. 2, 2021, p. 4. **6, 7**
- [44] X. Pan, P. Luo, J. Shi, and X. Tang, "Two at once: Enhancing learning and generalization capacities via ibn-net," in *European Conference on Computer Vision (ECCV)*, 2018, pp. 464–479. **7**
- [45] E. Ristani, F. Solera, R. Zou, R. Cucchiara, and C. Tomasi, "Performance measures and a data set for multi-target, multi-camera tracking," in *European Conference on Computer Vision*. Springer, 2016, pp. 17–35. **6**
- [46] L. Wei, S. Zhang, W. Gao, and Q. Tian, "Person transfer gan to bridge domain gap for person re-identification," in *IEEE Conference on Computer Vision and Pattern Recognition*, 2018, pp. 79–88. **6**
- [47] D. P. Kingma and J. Ba, "Adam: A method for stochastic optimization," in *3rd International Conference on Learning Representations*, 2015. **6**
- [48] Z. Zhong, L. Zheng, Z. Luo, S. Li, and Y. Yang, "Invariance matters: Exemplar memory for domain adaptive person re-identification," in *IEEE Conference on Computer Vision and Pattern Recognition*, 2019, pp. 598–607. **7**

- [49] Z. Wu, Y. Xiong, S. X. Yu, and D. Lin, "Unsupervised feature learning via non-parametric instance discrimination," in *IEEE Conference on Computer Vision and Pattern Recognition*, 2018, pp. 3733–3742. 7
- [50] J. Si, H. Zhang, C.-G. Li, J. Kuen, X. Kong, A. C. Kot, and G. Wang, "Dual attention matching network for context-aware feature sequence based person re-identification," in *Proceedings of the IEEE Conference on Computer Vision and Pattern Recognition*, 2018, pp. 5363–5372. 10
- [51] A. Dosovitskiy, L. Beyer, A. Kolesnikov, D. Weissenborn, X. Zhai, T. Unterthiner, M. Dehghani, M. Minderer, G. Heigold, S. Gelly, J. Uszkoreit, and N. Houlsby, "An image is worth 16x16 words: Transformers for image recognition at scale," *International Conference on Learning Representations*, 2021. 10
- [52] H. Sun, M. Li, and C.-G. Li, "Hybrid contrastive learning with cluster ensemble for unsupervised person re-identification," *arXiv preprint arXiv:2201.11995*, 2022. 10
- [53] X. Liu, W. Liu, H. Ma, and H. Fu, "Large-scale vehicle re-identification in urban surveillance videos," in *2016 IEEE international conference on multimedia and expo (ICME)*. IEEE, 2016, pp. 1–6. 10
- [54] X. Liu, W. Liu, T. Mei, and H. Ma, "Provid: Progressive and multi-modal vehicle reidentification for large-scale urban surveillance," *IEEE Transactions on Multimedia*, vol. 20, no. 3, pp. 645–658, 2017. 10